good fit to the formula. The VPI and SU CTS data (11.7 GHz) for the 1978 calendar year yielded $\tilde{a}$ - 41 dB and $\tilde{b}$ - 23.2 with R^2 = 0.95 when all data for CPA < 5dB is ignored. The UT data, covering about 18 months, gave $\tilde{a}$ = 41 dB, $\tilde{b}$ = 20.6 with R^2 = 0 99.

Figure 6.7-3 shows how the experimentally determined values of a and b for various frequencies and polarizations compare with the theoretically determined values from the formulas given previously. The theoretical predictions in general overestimate the depolarizing effects of the rain.

In the BTL experiment, co- and crosspolarized signal phase as well as amplitude was measured. This allowed the investigators to calculate XPD for arbitrary polarization states by vector manipulations. The beacon signal used, from a COMSTAR satellite, was linear polarized and oriented at about 21° from the local horizontal. Through the data conversion process, XPD versus CPA was determined on a statistical basis for linear polarization oriented O°, 45° and 90° from horizontal, and RHCP. Figure 4.3-5 shows the median 19 GHz curves for the true polarizations (21° from vertical and horizontal) and for vertical, horizontal and 45°. The experiment confirmed the theoretical result that maximum XPD occurs at 45°. Also, the XPD values calculated for RHCP were virtually identical to those at 45°, which is predicted by theory. The figure shows that the 21° curves fall between the 45° and the vertical/horizontal curves, and that XPD for horizontal polarization is greater than for vertical polarization. Both of these results aqree with physical reasoninq. A general aqreement with the XPD = $\tilde{a}$ - $\tilde{b}$ log CPA relation is evident for the lower three curves, in that they tend to lie near a straight line on the semilogarithmic plot. The CCIR approximation (4.3-27) is shown on the plot for the tilt angles 21° and 45°. In this case, the CCIR approximation appears to underestimate the depolarization.

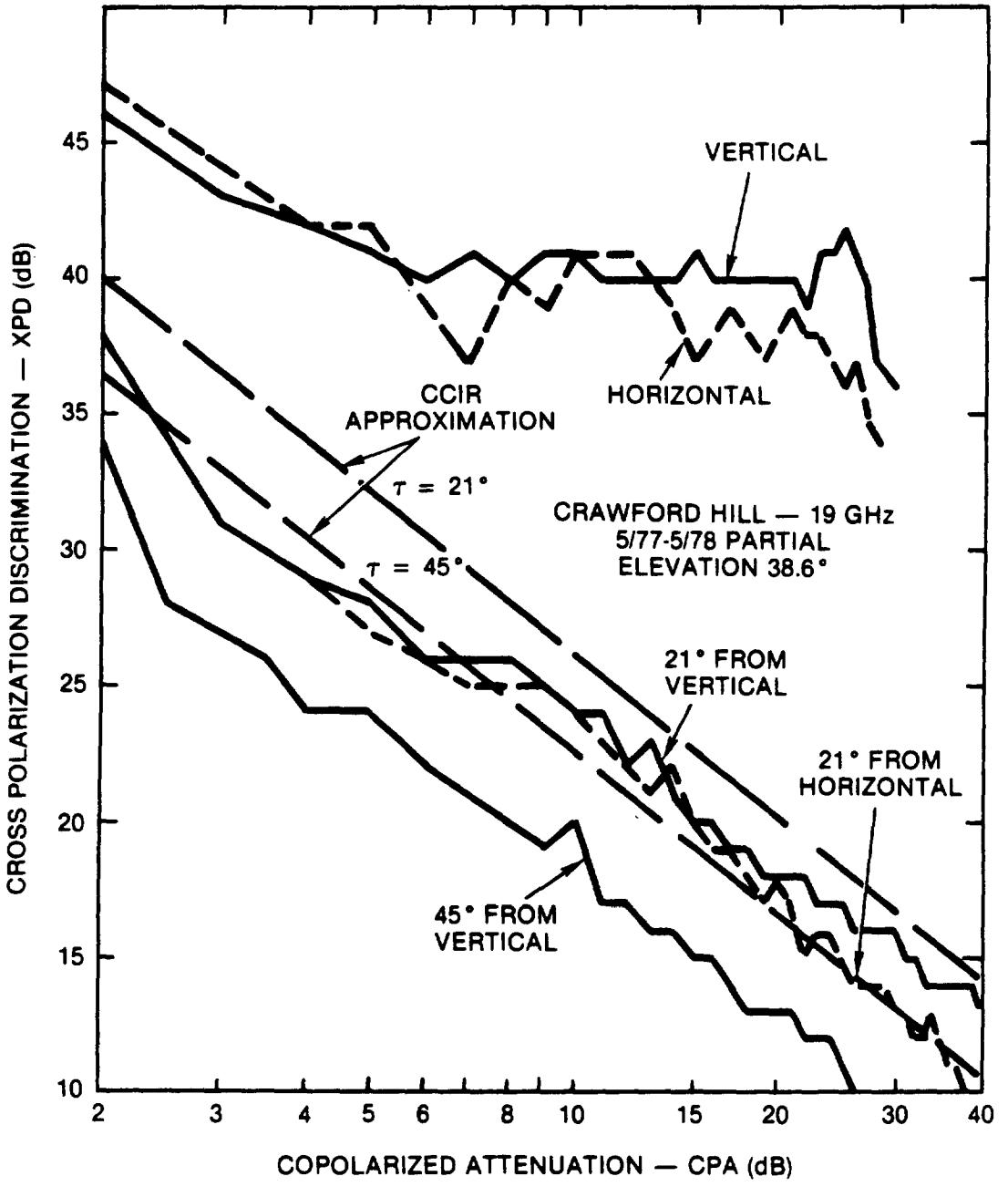

Figure 4.3-5. BTL COMSTAR Depolarization Experiment Results (Arnold, et.al. - 1979)

4.3.5 Phase of Crosspolarized Signal

Techniques have been developed for compensating for depolarization in dual-polarized satellite systems. They involve cancelling the crosstalk in one channel by inserting a properly levelled and phased sample of the opposite channel's signal. The signal sample used for cancelling must be exactly 180° out of phase from the crosspolarized signal for the technique to work. Its effectiveness depends, therefore, on how well the control system can determine and track the phase of the crosspolarized signal. This is a function of variability and rate of change of that phase.

Estimating the performance of crosstalk cancellation systems is one motivation for investigating crosspolarized signal phase. Another reason is that the signal phase is sensitive to certain properties of the rain medium (e.g. canting angle), and its measurement can aid in modelling the propagation properties of rain phenomena.

Overstreet and Bostian (1978) at VPI and SU derived a theoretical description of the phase between the copolarized and crosspolarized signals when rain depolarization is present. They assumed identically oriented raindrops, canted at an angle θ with respect to a copolarized reference direction, having known differential attenuation and phase and a known effective path length. Using Chu's differential attenuation and phase values for the frequencies and elevation angles of the CTS and COMSTAR D-2 beacons, they predicted the phase as a function of θ and rain rate, then found phase versus the XPD value for the same rain rate. The path lengths used were derived from attenuation statistics for those beacons at the VPI and SU station. For linearly polarized signals at 11 and 28 GHz, it was found that the phase was a fairly weak function of XPD and t , typically remaining with a 45° sector for XPD values down to 15 dB over the expected range of θ. For circular polarization, it was found that the phase difference Δ_c is given by

$$\Delta_c = \pm 2\theta + \Delta\ell(\theta = 45^\circ) \qquad (4.3\text{-}30)$$

where $\Delta\ell$ is the phase difference for LP waves, and the sign of the first term depends on whether RHCP or LHCP is copolarized. The LP phase difference at $\theta = 45^\circ$ is only weakly dependent on XPD so the 2θ term predominates in Δ_c.

Experimental data from the CP CTS beacon at 28.56 GHz generally confirmed the theoretical expectations. The phase difference of the LP signal normally remained in a 20-30° range during a rain depolarization event, whereas the CP signal phase difference varied widely during the course of a rain event. The phase versus XPD changes generally followed a characteristic sequence during convective storms. This indicated the changes in the nature of the depolarizing medium, primarily in predominant canting angle of the raindrops present, through the passage of the storm cell.

The experimental evidence suggests that crosstalk cancellation schemes would be more effective using LP than CP waves. The phase of the crosspolarized signal, which must be estimated by the cancellation system, is much less variable with linear polarization. In fact, setting the phase of the cancellation signal to a constant value would give a degree of effectiveness, while eliminating the need for a complex phase shifter control system.

4.3.6 Rate of Change of Depolarization

To more fully characterize depolarization, some quantitative description of the rate of change of the amplitude and phase of the crosspolarized signal would be desirable. This information would assist us in designing adaptive controls for crosstalk cancellation systems, and may also provide further insight into the nature of the meteorological process responsible for depolarization. However, there has apparently been little research effort expended to this end. Further experimental work, or further analysis of existing data bases, is needed in this area.

4.3.7 Rain Depolarization Dependence on Elevation Angle and Frequency

Knowledge of the dependence of crosspolarization discrimination on elevation angle and frequency is quite valuable because it allows us to extend the usefulness of time-consuming and costly measurements. Unfortunately, the present limited body of experimental evidence does not overwhelmingly support the theoretical scaling relations, so they must be used with caution.

The expression obtained earlier for XPD (eq. 4.3-16),

$$XPD = -20 \log \left[\frac{1}{2} m_\theta L |\Delta k'| \cos^2\varepsilon \sin 2\bar{\theta}\right] \qquad (4.3\text{-}31)$$

can be rewritten to explicitly show the elevation angle and frequency dependencies. For the CP case, corresponding to the minimum XPD, we have $\bar{\theta} = 45^\circ$ which gives

$$\begin{aligned} XPD = & -20 \log (L \cos^2\varepsilon) \\ & -20 \log |\Delta k'| \\ & -20 \log (m_\theta/2) \end{aligned} \qquad (4.3\text{.-}32)$$

Using the empirical relations (Nowland, et al-1977):

$$\begin{aligned} L &= [7.41 \times 10^{-3} R^{0.766} + (0.232 - 1.8 \times 10^{-4} R) \sin \varepsilon]^{-1} \\ |\Delta k'| &\cong c(f)\, R^{d(f)} \end{aligned} \qquad (4.3\text{-}33)$$

It is apparent that the first term in the XPD expression is a function of rain rate and elevation angle only, and the second term is a function of rain rate and frequency only. These terms are plotted in Figure 4.3-6. The last term can be considered constant, though it may also be a function of rain rate. For $m_\theta = 0.8$, the last term is 8 dB.

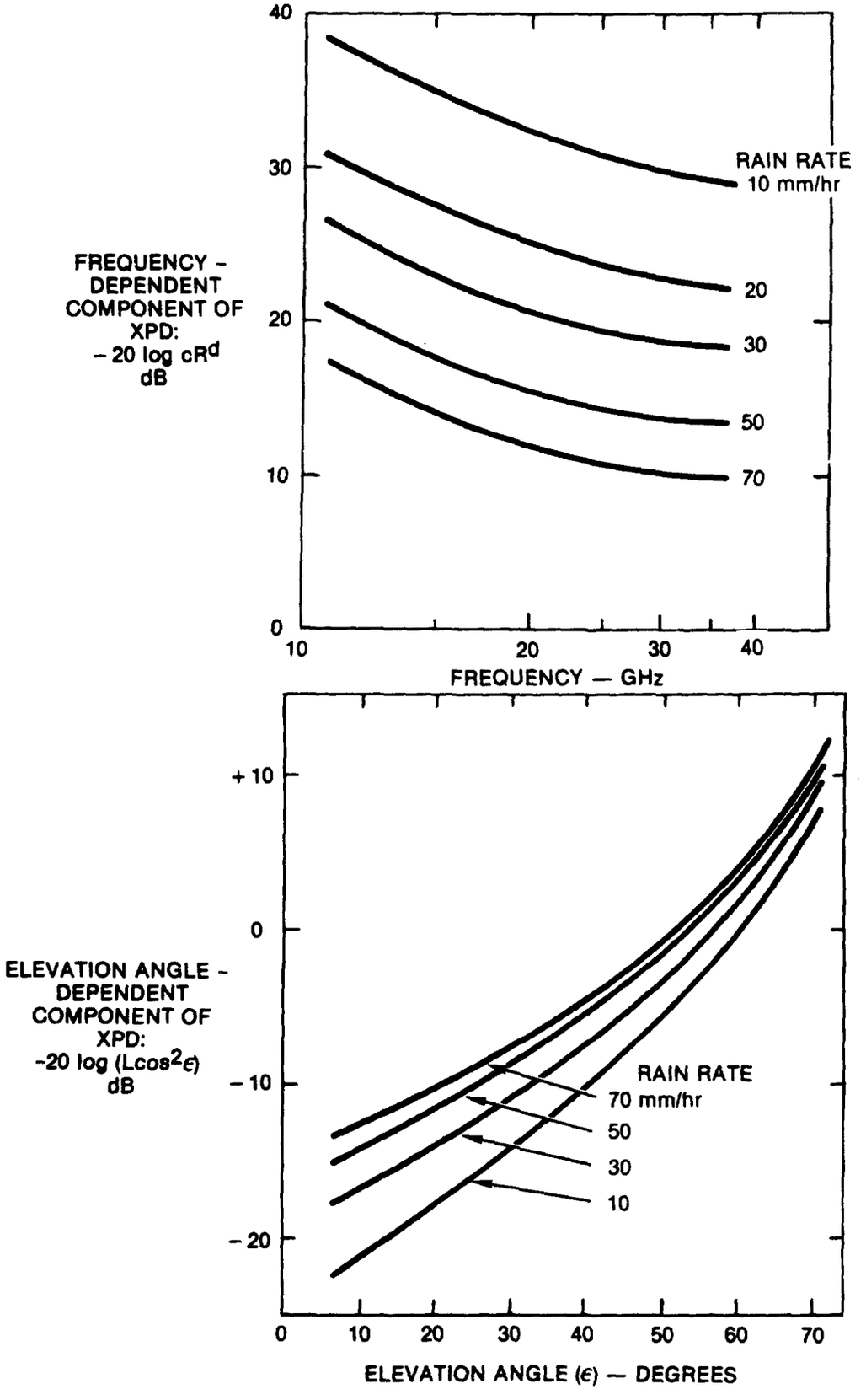

Figure 4.3-6. Frequency and Elevation Angle Dependence of XPD for CP

Another depiction of the frequency dependence of XPD is shown in Figure 4.3-7. It shows the predicted XPD vs CPA relations for fixed frequencies and elevation angle. It is clear that, for any given rain rate, both CPA and XPD get worse as frequency increases. However, for a given value of CPA, XPD improves with frequency.

4.4 ICE DEPOLARIZATION

The second major cause of depolarization on Earth-space paths, besides rain, is the presence of ice crystals in clouds at high altitudes. Ice crystal depolarization is different from rain depolarization in that it is not accompanied by appreciable copolarized attenuation. This is because the depolarization is caused primarily by differential phase shifts, rather than differential attenuation, which is responsible for rain depolarization. Another distinguishing characteristic is that the amplitude and phase of the crosspolarized signal often undergo abrupt, coincident changes with large excursions.

4.4.1 Meteorological Presence of Ice

Clouds present above the freezing level consist, completely or in part, of ice crystals. Cirrus clouds, and the "anvil" that forms at the top of mature thunderstorms are all ice, and the upper parts of cumulonimbus clouds are predominately ice. The crystals that are present have one of two shapes determined by the temperature at the time of formation. Very cold temperatures, below about -25°C, favor the formation of needle-shaped crystals. Flat, plate-like crystals form in a moderately cold environment (-9° to -25°C). The dimensions of the crystals vary between about 0.1 and 1 mm.

Ice crystals form on dust particle nuclei in the atmosphere. The relative abundance of dust particles has been hypothesized as the reason for differences observed in ice depolarization at different locations. In maritime regions, the air contains relatively few dust particles compared with continental areas. As a result of this, maritime air tends to have fewer, but larger ice

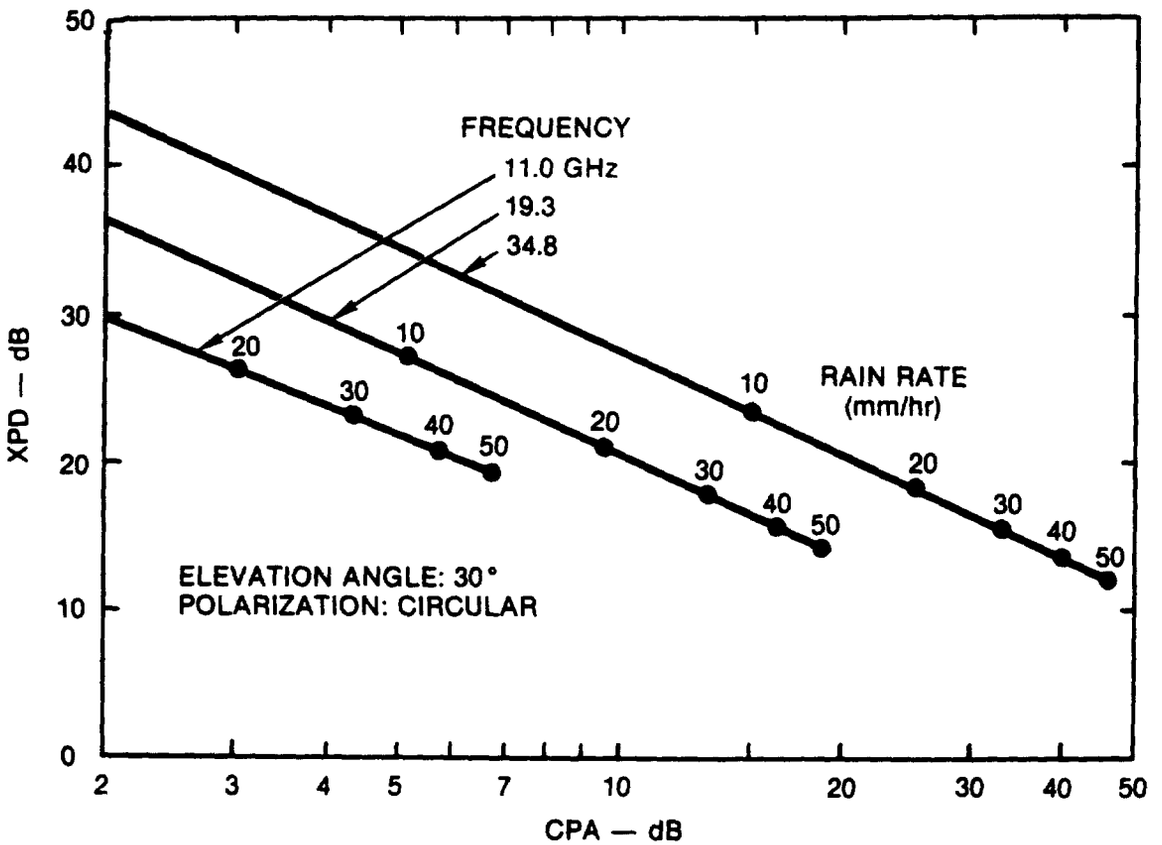

Figure 4.3-7. Frequency and Rain Rate Dependence of XPD and CPA

particles than continental air under similar conditions. It is believed that the presence of larger crystals accounts for the generally higher values of XPD observed in maritime versus inland locations (i.e., BTL versus VPI & SU).

Like raindrops, ice crystals are non-symmetrical and they have a dielectric constant much different from air. These are two of the necessary conditions for depolarization. A third condition, a preferred particle alignment, is also required. Oblate raindrops are aligned by aerodynamic forces, and their preferred alignment direction is affected by the prevailing winds. Aerodynamics also plays a role in aligning ice particles, but it is believed electrostatic forces also play a large part. This belief is supported by many observations during thunderstorms of rapid XPD changes coinciding with lightning flashes. This coincidence may be explained by the following: Electric fields present in regions between oppositely-charged clouds exert torques on the highly non-symmetrical ice crystals. When the field is sufficiently strong, these torques become significant in comparison with the turbulent aerodynamic forces, resulting in an average alignment of the "needle" crystal axes and the "plate" crystal planes along the direction of the field lines. When a lightning discharge takes place between the clouds, charges are equalized and the electric field intensity drops. Aeroydnamic forces then predominate, and the crystals quickly lose their preference for a particular direction of orientation (Bostian and Allnut - 1979).

4.4.2 Model for Ice Depolarization

Propagation through a region containing ice crystals can be analyzed in a manner analogous to that applied to rain. In the case of ice, the crystals are modelled as highly eccentric prolate spheroids ("needle" crystals) or oblate spheroids ("plate" crystals). Haworth, Watson and McEwan (1977) have performed this analysis. They assumed that due to aerodynamic forces, the "plate" crystals were oriented horizontally and the axes of the "needle" crystals stayed in the horizontal plane. Under this assumption, an

electrostatic field has no effect on "plates", and aligns the "needles" along the horizontal component of the field. Figure 4.4-1 shows the magnitude of the predicted ice XPD. The "needle"-produced XPD varies with ϕ, the average orientation angle of the crystal axes measured in the horizontal plane. The parameter α is a measure of the degree of alignment of the crystal axes. When the axes are uniformly distributed in all directions, $\alpha = 0$, and when all crystals are oriented in the same direction, $\alpha = 1$.

The phase of the crosspolarized signal, as predicted by the model, undergoes an abrupt change of 180° as $\bar{\phi}$ passes through the values corresponding to the XPD peaks,(crosspolarized signal nulls). These are at 80° and 130° in the figure. When α is below some critical value, however, (falling between 0.5 and 1.0 for the example shown) the double null and accompanying phase jump don't occur. This phase reversal phenomenon has been observed at the time of lightning flashes in thunderstorms (see Figure 6.7-8) and is accompanied by a jump in XPD amplitude. Bearing the earlier discussion in mind, we would expect changes in α and $\bar{\phi}$ to accompany lightning discharges. The same behavior has also been detected during the passage of non-electrically-active clouds (Shutie, et al-1978). This implies that a particular mechanism, probably wind shear, is responsible for crystal alignment, besides electrostatic fields.

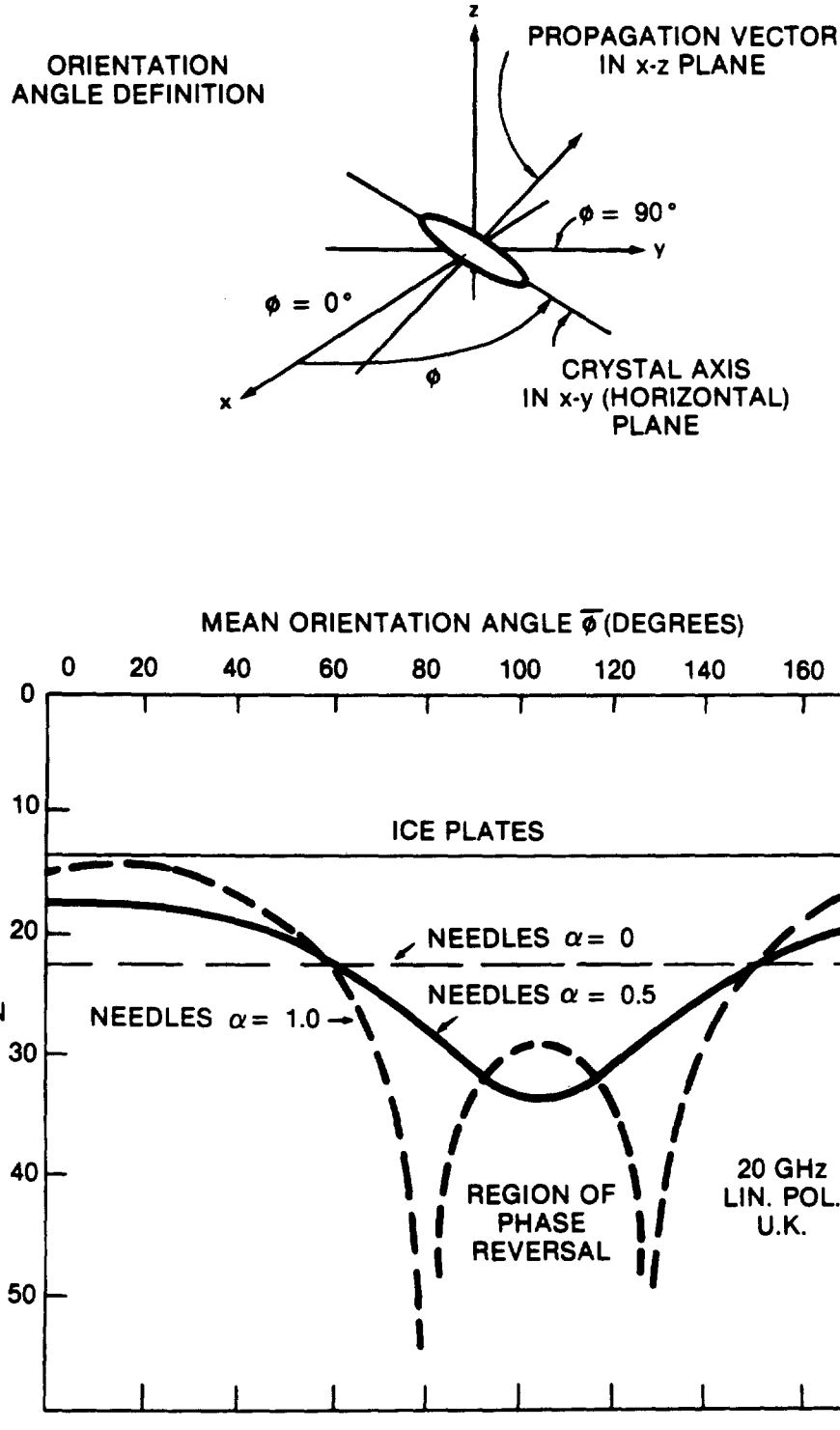

Figure 4.4-1. Definition of Orientation Angle φ and Predicted XPD (From Bostian and Allnut, 1979)

4.5 REFERENCES

Arnold, H.W. et al (1979), "Characteristics of Rain and Ice Depolarization for a 19 and 28 GHz Propagation Path from a Comstar Statellite," Record, Int'l Conf. on Communications.

Bostian, C.W. and J.E. Allnut (1979), "Ice-Crystal Depolarization on Satellite-Earth Microwave Radio Paths," Proc. IEE, Vol. 126, p. 951.

Bostian, C.W. and J.R. Dent (1979), "CTS 11.7 GHz Isolation Data for the Calendar Year 1978," VPI & SU Report, prepared for NASA under Contract No. NAS5-22577.

CCIR (1977), Document 5/206 (Canada), "Techniques for the Prediction of Rain Depolarization Statistics at Microwave and Millimeter Wavelengths."

CCIR (1978), "Propagation Data Required for Space Telecommunications Systems," Report 564-1, in Volume V, Recommendations and Reports of the CCIR - 1978, International Telecommunications Union, Geneva.

CCIR (1986), "Propagation Data and Prediction Methods Required for Space Telecommunications Systems," Report 564-3, in Volume V, Recommendations and Reports of the CCIR - 1986, International Telecommunications Union, Geneva.

Chu, T.S. (1974), "Rain-Induced Cross-Polarization at Centimeter and Millimeter Wavelengths," Bell Syst. Tech. Jrnl, Vol. 58, No. 8, pp. 1557-1579.

Chu, T.S. (1980), "Microwave Depolarization of an Earth-Space Path," BSTJ, Vol. 59, No. 6 (July-Aug) pp. 987-1107.

Chu, T.S. (1982), "A Semi-Empirical Formula for Microwave Depolarization Versus Rain Attenuation on Earth-Space Paths, "IEEE Trans. on Communications, Vol. COM-30, No. 12, (Dec) pp 2550-2554.

Haworth, D.P., P.A. Watson, and N.J. McEwan (1977), "Model for the Effects of Electric Fields on Satellite-Earth Microwave Radio Propagation," Elect. Letters, Vol. 13, p. 562.

Hendry, A., G.C. McCormick and B.L. Barge (1976), "Ku-Band and S-Band Observations of the Differential Propagation Constant in Snow," IEEE Trans. Ant. Prop., Vol. AP-24, No. 4, pp. 521-525.

Kanellopoulos, J.D. and R.H. Clarke (1981), "A Method of Calculating Rain Depolarization Distributions on Microwave Path," Radio Science, Vol. 16, No. 1 (Jan-Feb), pp. 55-65.

McCormick, G.C. and A. Hendry (1977), "Depolarization by Solid Hydrometeors," Electronics Letters, Vol. 13, No. 3.

Morrison, J.A., M.J. Cross, and T.S. Chu (1973), "Rain-Induced Differential Attenuation and Differential Phase Shift at Microwave Frequencies," BSTJ, Vol. 52, No. 4, pp. 599-604.

Nowland, W.L., R.L. Olsen, and I.P. Shkarofsky (1977), "Theoretical Relationship Between Rain Depolarization and Attenuation," Electronics Letters, Vol. 13, No. 22, pp. 676-677.

Oguchi, T. (1977), "Scattering Properties of Pruppacher-and-Pitter Form Raindrops and Cross Polarization Due to Rain: Calculations at 11, 13, 19.3 and 34.8 GHz," Radio Science, Vol. 12, pp. 41-51.

Pruppacher, H.R. and R.L. Pitter (1971), "A Semi-empirical Determination of the Shape of Cloud and Rain Drops," J. Atmos. Science, Vol. 28, pp. 86-94.

Shutie, P.F., E.C. MacKenzie and J.E. Allnut (1978), "Relative Phase Measurements at 30 GHz Between Copolar and Induced Crosspolar Signals Produced by Ice Particles on a Satellite-to-Ground Link," Elect. Letters, Vol. 14, No. 4, p. 105.

Stutzman, W.L. (1977), "Mathematical Formulations and Definitions for Dual Polarized Reception of a Wave Passing Through a Depolarizing Medium (A Polarization Primer)," Virginia Polytechnic Institute & State Univ. Report, prepared under NASA Contract NAS5-22577.

Stutzman, W.L., C.W. Bostian, A. Tsolakis, and T. Pratt, (1983), "The Impact of Ice Along Satellite-to-Earth Paths on 11 GHz Depolarization Statistics," Radio Science, Vol. 18, No. 5, pp. 720-724.

Thomas, D.T. (1971), "Cross-Polarization Distortion in Microwave Radio Transmission Due to Rain," Radio Science, Vol. 6, No. 10, pp. 833-839.

Vogel, W.J. (1978), "CTS Attenuation and Cross-Polarization Measurements at 11.7 GHz," Final Report, Elect. Eng. Res. Lab., Univ. Texas at Austin, prepared under NASA Contract NAS5-22576.

Wallace, R.G. (1981), "Site Diversity Effects on Communication Satellite System Availability," ORI Technical Report 1891, prepared for NASA Headquarters under Contract NASW-3436.

Watson, P.A., and M. Arbabi (1973a), "Rainfall Crosspolarization at Microwave Frequencies," Proc. IEE, Vol. 120, No. 4, pp. 413-418.

Watson, P.A., and M. Arbabi (1973b), "Cross-Polarization Isolation and Discrimination," Electronics Letters, Vol. 9, N. 22, pp. 516-519.

CHAPTER V

PROPAGATION DATA BASES

Researchers have been performing experiments to gather propagation data on millimeter-wave Earth-space links since the late 1960's, and in the process, have accumulated sizable data bases. In this chapter, we describe the various satellites used in this work, and present summary results of the significant experiments conducted in the United States. The results presented are primarily cumulative attenuation statistics, though some depolarization measurements are included as well. This is, by necessity, a limited sampling of the existing data bases. We therefore preface the data by citing additional summaries of propagation data for the interested reader.

5.1 SUMMARIES OF EXPERIMENTAL DATA

The International Radio Consultative Committee (CCIR) publishes a summary of worldwide experimental data in the Recommendations and Reports issuing from its periodic plenary assemblies. Volume V of this publication, "Propagation in Non-Ionized Media," deals with all aspects of microwave propagation--both terrestrial and earth-to-space. Within Volume V, the data is presented as a series of reports and recommendations submitted to and adopted by the CCIR. Because of this presentation format, data of interest to designers may be found in several places.

The most complete collection of measured propagation data is found in the two CCIR documents;

1. Report 564-3, "Propagation Data and Prediction Methods Required for Earth-Space Telecommunications Systems," (CCIR-1986a), and

2. Document 5/378, "Data Banks Used for Testing Prediciton Methods in Sections E, F and G of Volume V," (CCIR-1986b).

The CCIR separates the data between the two reports based on the availability of an acceptable prediction method for that type of measurement. Data for which an accepted method does not exist is presented in the first document (Report 564-3), while data for which an accepted method does exist is presented in the second document.

The data summaries in Report 564-3 are presented in Annex I, and include sections on the following subjects:

- Seasonal variations - worst month
- Duration of individual fades
- Rates of change of attenuation
- Scintillation and multipath effects
- Noise temperature
- Cross-polarization due to hydrometeors
- Angle-of-arrival

Document 5/378 presents detailed tabulations of earth-space path data for:

- Annual slant-path rain attenuation statistics (Table II-1),
- Worst month slant-path attenuation statistics (Table II-2),

- Fade duration statistics (Table II-3), and
- Annual XPD statistics based on satellite measurements (Table II-4).

The results of extensive NASA sponsored measurements conducted in the 1970's is documented in a report entitled "A Compendium of Millimeter Wave Propagaiton Studies Performed by NASA," (Kaul, et al - 1977). The report contains a reasonably complete summary and references to the 15.3 and 31.65 GHz measurements with ATS-5, and the 13.2, 17.8, 20 and 30 GHz measurements with ATS-6.

5.2 SATELLITES USED FOR PROPAGATION RESEARCH

Within the United States and Canada, four satellite systems (seven satellites) have been utilized to obtain the bulk of the earth-space propagation data. A brief summary of the satellite characteristics that relate to propagation studies is given in Table 5.2-1.

European researchers used 20 and 30 GHz transmissions from the ATS-6 during the 1975/76 period when the satellite was stationed over Europe. The Italian satellite SIRIO, carrying a circularly polarized three-carrier beacon at 11.331, 11.597 and 11.836 GHz, began operation in October 1977. Finally, the Orbiting Test Satellite (OTS), launched by the European Space Agency, provided beacon transmissions at 11.575 and 11.786 GHz starting in May 1978. The Japanese have launched four satellites supporting propagation research. These are designated ETS-II, CS, BS and ECS, and carry beacons at various frequencies near 12, 20 and 34 GHz (Hayashi, et al-1979).

Satellite propagation beacons are not the only means for collecting experimental data. Radars, radiometers (fixed and sun synchronous) and low-orbiting satellites can also provide valuable data, but usually with some deficiency. A general deficiency is the lack of polarization data available from these measurement

Table 5.2-1. Satellite Parameters Related to Propagation Studies

Satellite	Launch Date	Satellite Position	Uplink Frequencies	Downlink Frequencies	Antenna
ATS-5	8/12/69	Initially over Indian Ocean, drifted to 108° W. longitude; remained spinning at 76 rpm	31.65 GHz with sidebands at ±1, ±10, and ±50 MHz from carrier	15.3 GHz with sidebands at ±0.1, ±1, ±50 MHz from carrier	Linearly polarized conical horns with 20° coverage and 19.1 dB boresight gain
ATS-6	5/30/74	94° W. longitude for first year then move to 35° E. long. and returned to 140° W.	COMSAT Exp.: 13.19 - 13.2 GHz 17.74 - 17.8 GHz	COMSAT Exp.: 4.14 - 4.15 GHz 4.16 - 4.17 GHz NASA/GSFC Exp.: 20 and 30 GHz 8 sidetones Spaced ±180 MHz	COMSAT Exp.: Dual-frequency linearly polarized dish NASA/GSFC Exp.: 20 GHz: 6° x 9° horn 2° dish 30 GHz: similar to above
CTS	1/17/76	116° W.	14.0 - 14.5 GHz	11.7 GHz beacon 11.7 - 12.2 GHz	16° horn, RHCP for beacon
COMSTAR (satellites D1, D2, D3 and D4)	D1: 5/13/76 D2: 7/22/76 D3: 6/29/78 D4: 2/21/81	D1: 95° W. long. D2: 95° W. long. D3: 87° W. long. D4: 127° W. long.	5.9 - 6.4 GHz	19.04 and 28.56 GHz beacons 3.9 - 4.2 GHz	Linearly polarized offset parabolic dishes. 19.04 GHz switched between vertical and horizontal polarization. 28.56 GHz vertically polarized. Sidebands of 28.56 GHz ±528.9 MHz (D3) ±264.4 MHz (D1 and D2)
ETS-II	2/77	130° E. long.		1.7, 11.5, 34.5 GHz beacons	
SIRIO	8/77	15° W. long.	17.4 GHz	11.3, 11.6, 11.9 GHz beacons	
CS	12/77	135° E. long.	27.6 - 6.3 GHz 6.0 - 6.3 GHz	3.95, 19.45 GHz beacons 17.9 - 20.2 GHz 3.8 - 4.1 GHz	
BS	4/78	110° E. long.	14.0 - 14.4 GHz	11.7 GHz beacon 12.0 - 12.1 GHz	
OTS	5/78	10° E. long.	14.2 - 14.5 GHz	11.6 - 11.8 GHz beacons 11.5 - 11.8 GHz	

techniques. Specifically, the expense of calibrating and operating radar systems and the attenuation saturation effect in radiometer systems limit their use.

5.3 FORMAT OF DATA PRESENTED

Because of the volume and variety of data being presented by experimenters throughout the United States and Canada, it is impossible to claim that the following data is complete. However it is certainly representative of the tropospheric effects on earth-space paths for the location indicated.

To limit the volume of data presented, the cumulative attenuation statistics will be emphasized, since this is the most complete data base available and, from this, the rain rate and depolarization may be inferred (as described in Chapters 3 and 4). The results will be presented by frequency range or satellite beacon frequency, as appropriate.

To assist with the comparison of data from various experimenters, NASA has encouraged the use of standardized cumulative statistics plot formats. The use of these formats, given in Figures 5.3-1 and 5.3-2, will permit experimental results from different sources to be overlaid for direct comparison. The forms cover from 0.0001 to 10 percent of the total period, which should be a sufficiently large range for most applications. The attenuation scales cover from 0-35 and 0-45 dB, which should be sufficient to cover the link margin range of most systems. The 45 dB graph is recommended for use above 15 GHz. These same forms may be utilized for depolarization statistics if the attenuation labels are changed to cross-polarization discrimination. Each chart should be labeled with the period of the measurement, frequency, location and elevation angle. This provides, on the figure, all the information needed for comparison of data.

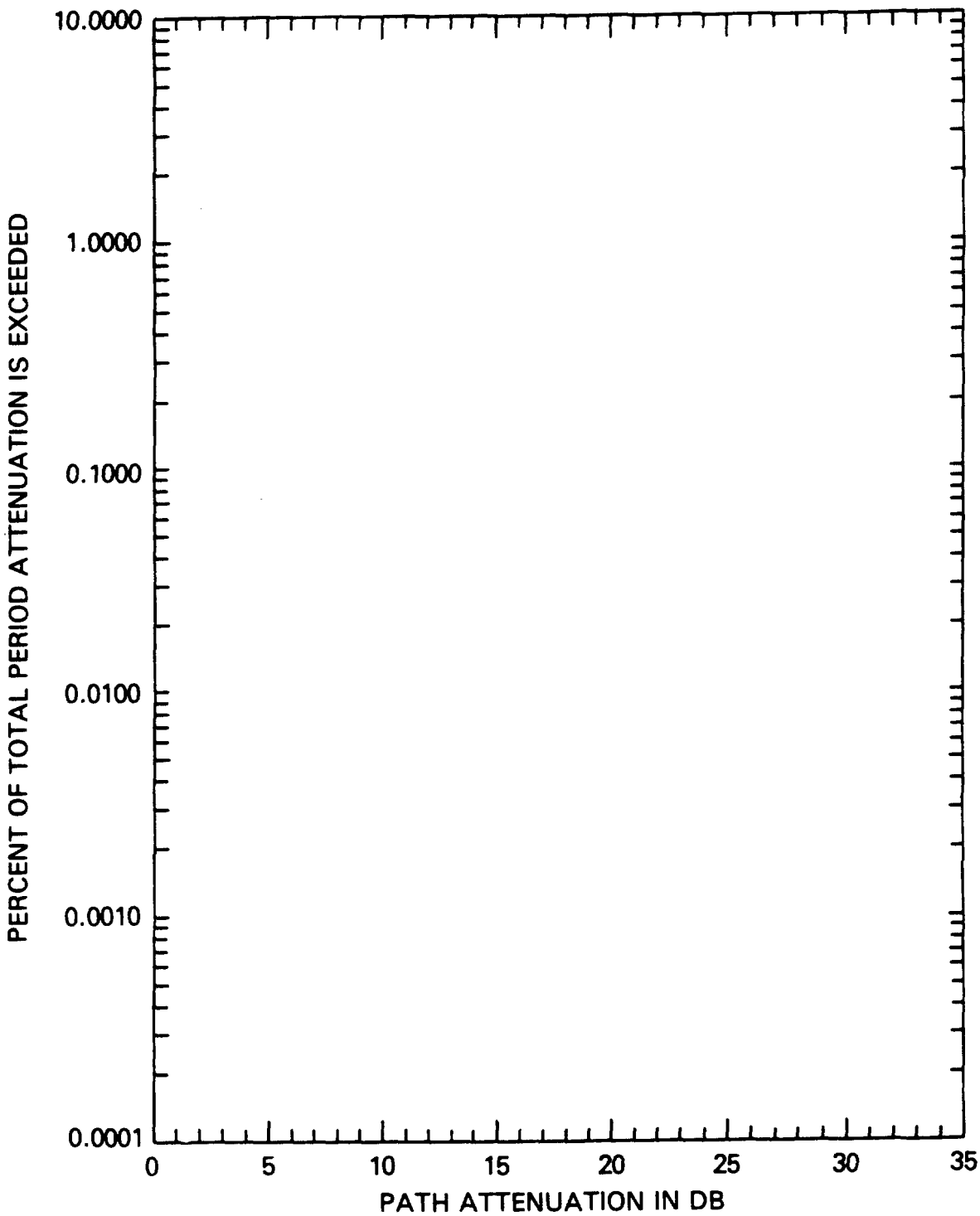

Figure 5.3-1. Cumulative Attenuation Graph for Use in the 11/14 GHz Bands

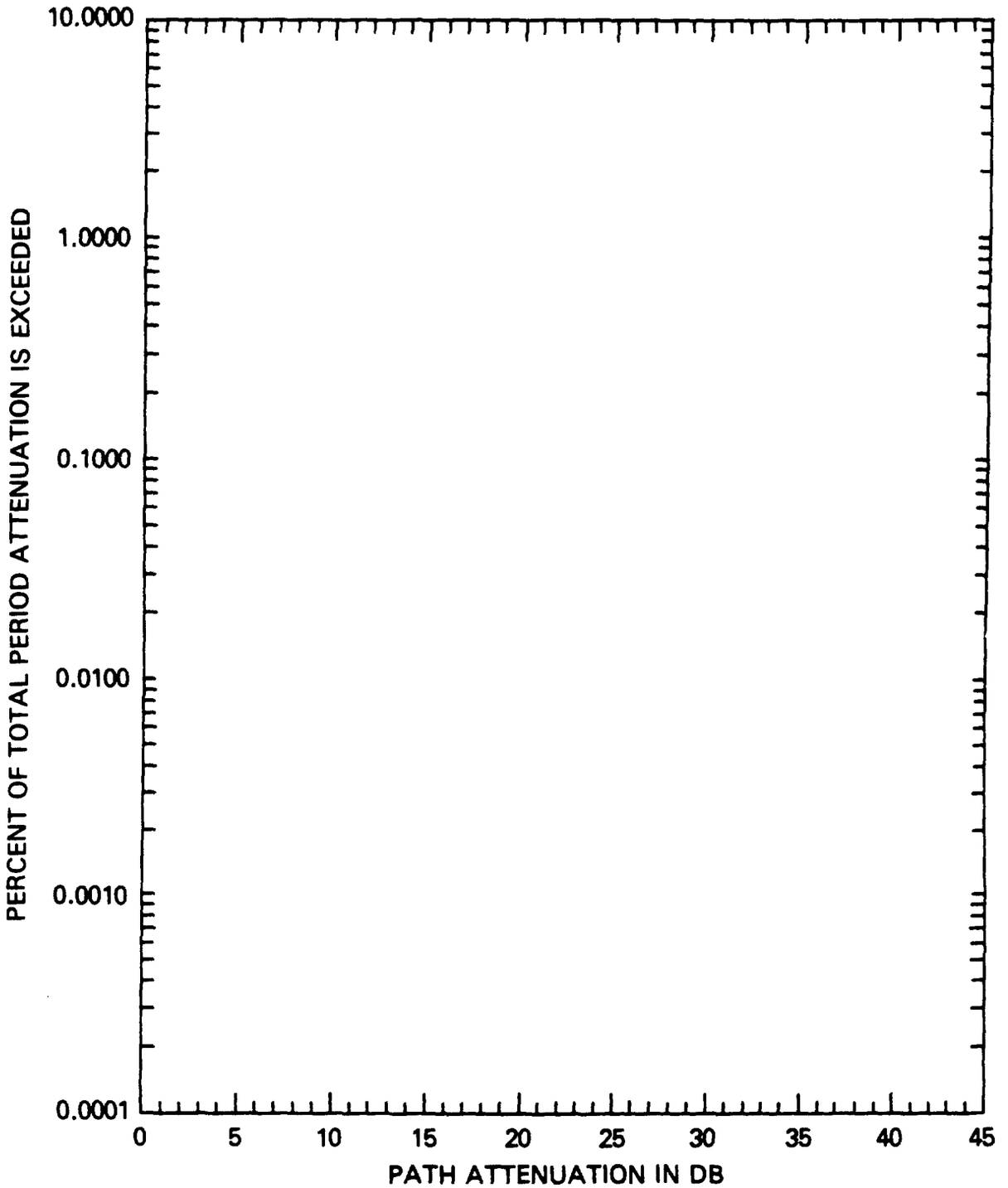

Figure 5.3-2. Cumulative Attenuation Graph for Use above 15 GHz

5.4 EXPERIMENTAL CUMULATIVE ATTENUATION STATISTICS

5.4.1 11.5-11.7 GHz Data

The Communications Technology Satellite (CTS) has provided the opportunity for extensive long-term measurements of rainfall attenuation and other propagation effects in the 11.7 to 12.2 GHz band. A continuous 11.7 GHz circularly polarized beacon operated from launch through late 1979, except for two periods during solar eclipse (March 4 through April 16, 1976 and August 31 through October 17, 1976).

Figures 5.4-1 through 5.4-5 show the cumulative statistics for the five United States locations of (listing in order of ascending elevation angle):

Waltham, MA (GTE Laboratories, Inc.)

Holmdel, NJ (Bell Telephone Labs.)

Greenbelt, MD (NASA Goddard Space Flight Center)

Blacksburg, VA (Virginia Polytechnic Institute and State University)

Austin, TX (University of Texas at Austin)

All of the distributions are based on 12 calendar months of continuous data. Details of the recording methods and processing techniques are given in the references in each figure. Table 5.4-1 summarizes the attenuation statistics at each of the locations for 0.001, 0.005, 0.01, 0.05, 0.1, 0.5 and 1% of the observation period. Note that the data shows a wide range of variations, even for consecutive years at one location.

Elevation angle differences between the five locations prevents a direct comparison of the measured distributions. The distributions can be converted to a common elevation angle by assuming the precipitation to be horizontally stratified in the

Table 5.4-1. Annual 11.7 GHz Attenuation Statistics Summary

LOCATION	ELEVATION ANGLE	TIME PERIOD	ATTENUATION (dB) FOR GIVEN PERCENT OUTAGE						
			1%	0.5%	0.1%	0.05%	0.01%	0.005%	0.001%
Waltham, MA	24°	Feb '77 - Jan '78	<1	<1	2.5	4	10.5	14.5	(23)
		Feb '78 - Jan '79	<1	<1	1.5	2.8	8.5	11	15.3
Holmdel, N.J.	27°	Jun '76 - Jun '77	<1	<1	3	5	13.5	-	-
		Jun '77 - Jun '78	<1	<1	3	5	13.5	19.5	-
		Jun '78 - Jun '79	<1	<1	2.5	3.8	9.2	12.2	29
Greenbelt, MD	29°	Jul '76 - Jun '77	<1	<1	1.8	3.2	8.8	14.5	>30
		Jul '77 - Jun '78	<1	1	2.1	3.8	12	18	26.4
		Jul '78 - Jun '79	<1	<1	1.8	3.2	14	21	29.2
Blacksburg, VA	33°	Jan '77 - Dec '77	2	2.5	4	5	13	16.5	24
		Jan '78 - Dec '78	2	2.7	3.7	4.3	6.8	8.6	13
Austin, TX	49°	Feb '78 - Jan '79	<1	1	3	5.5	13	18	23

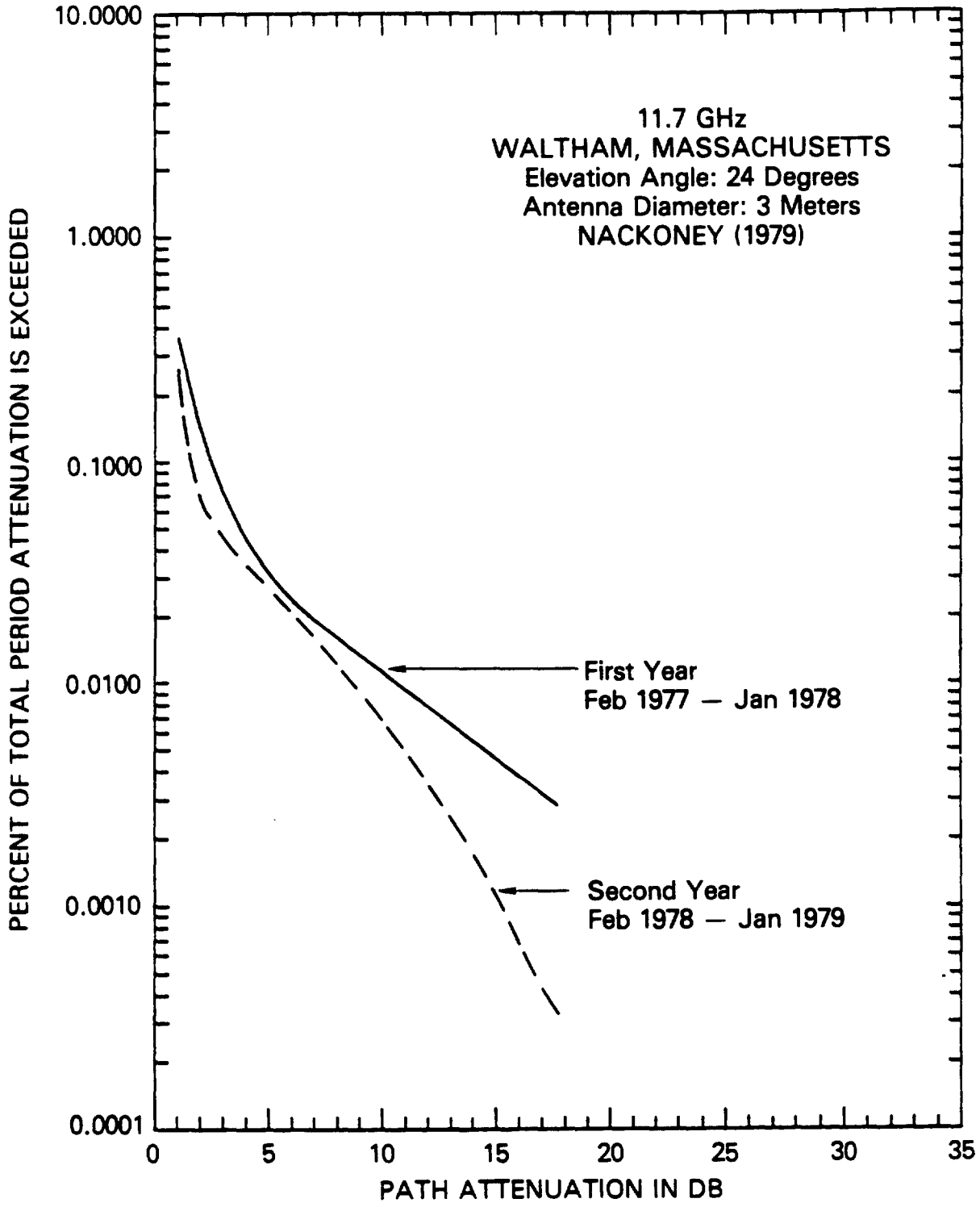

Figure 5.4-1. Annual 11.7 GHz Attenuation Distributions for Waltham, MA

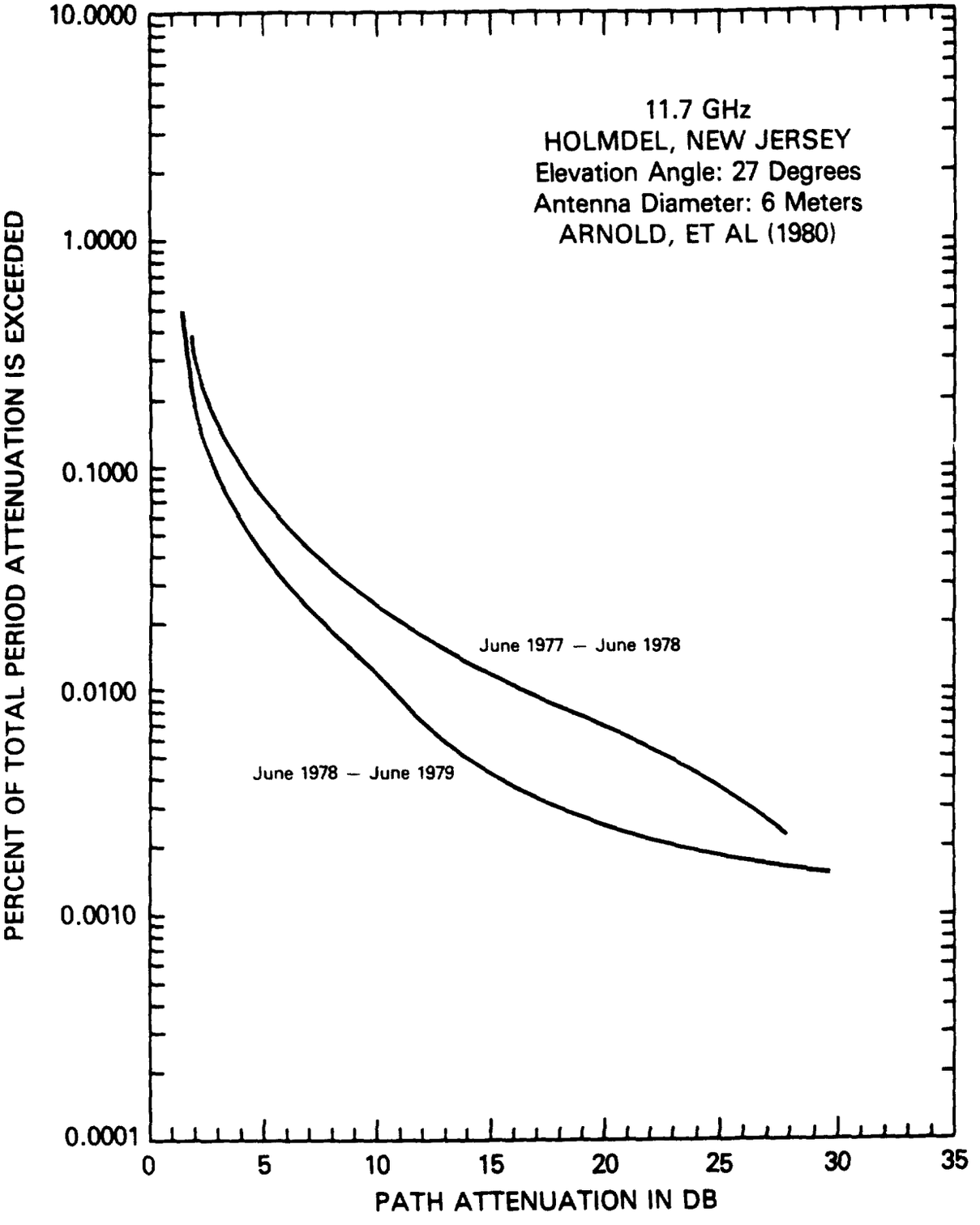

Figure 5.4-2. Anual 11.7 GHz Attenuation Distribution for Holmdel, NJ